Six-circle diffractometer with atmosphere- and temperature-controlled sample stage and area and line detectors for use in the G2 experimental station at CHESS

D. E. Nowak
Department of Materials Science and Engineering, Cornell University, Ithaca, New York 14853

D. R. Blasini
Department of Chemistry and Chemical Biology, Cornell University, Ithaca, New York 14853

A. M. Vodnick
Department of Materials Science and Engineering, Ithaca, Cornell University, New York 14853

B. Blank
Advanced Design Consulting USA, Inc., Lansing, New York 14882 and SpaceMill Sciences Corp., Freeville, New York 13068

M. W. Tate
Department of Physics, Ithaca, Cornell University, New York 14853

A. Deyhim
Advanced Design Consulting USA, Inc., Lansing, New York 14882

D.-M. Smilgies
Cornell High Energy Synchrotron Source, Wilson Laboratory, Ithaca, New York 14853

H. Abruña
Department of Chemistry and Chemical Biology, Cornell University, Ithaca, New York 14853

S. M. Gruner
Department of Physics, Cornell University, Ithaca, New York 14853 and Cornell High Energy Synchrotron Source, Wilson Laboratory, Ithaca, New York 14853

S. P. Baker
Department of Materials Science and Engineering, Cornell University, Ithaca, New York 14853

(Received 18 May 2006; accepted 17 July 2006; published online 14 November 2006)

A new diffractometer system was designed and built for the G2 experimental station at the Cornell High Energy Synchrotron Source (CHESS). A six-circle κ goniometer, which provides better access to reciprocal space compared to Eulerian cradles, was chosen primarily to perform large angle Bragg diffraction on samples with preferred crystallographic orientations, and can access both horizontal and vertical diffraction planes. A new atmosphere- and temperature-controlled sample stage was designed for thin film thermomechanical experiments. The stage can be operated in ultrahigh vacuum and uses a Be dome x-ray window to provide access to all scattering vectors above a sample's horizon. A novel design minimizes sample displacements during thermal cycling to less than 160 μm over 900 °C and the stage is motorized for easy height adjustments, which can be used to compensate for displacements from thermal expansion. A new area detector was built and a new line detector was purchased. Both detectors cover a large region in reciprocal space, providing the ability to measure time-resolved phenomena. A detailed description of the design and technical characteristics is given. Some capabilities of the diffractometer system are illustrated by a strain analysis on a thin metal film and characterization of organic thin films with grazing incidence diffraction. The G2 experimental station, as part of CHESS, is a national user facility and is available to external users by application. © *2006 American Institute of Physics.*
[DOI: 10.1063/1.2372730]

I. INTRODUCTION

A very capable general-purpose diffractometer system has been added to the G2 experimental station, a shared user facility supported by the National Science Foundation, at the Cornell High Energy Synchrotron Source (CHESS). The new diffractometer system was designed to be as flexible as possible and can easily be adapted to work with a wide range of experimental setups. The new system features a six-circle diffractometer, an atmosphere- and temperature-controlled sample stage, and area and line detectors.

The range of experiments that are possible using this equipment can be illustrated by two sets of measurements for which it was explicitly designed: thin film thermomechanical

experiments using x-ray diffraction strain analysis methods[1–4] and surface sensitive scattering experiments using grazing incidence-reciprocal space mapping (GI-RSM).[5] Thermomechanical tests[6,7] have been developed to measure thin film mechanical properties because thin films are usually adhered to substrates and traditional mechanical testing techniques, such as uniaxial tensile testing, typically cannot be used. In thermomechanical tests, the difference in thermal expansion coefficients between a film and substrate is used to generate a strain in the film by changing the temperature. Typically, the temperature is changed incrementally and then held constant while multiple Bragg diffraction peaks are measured. Strains are determined from shifts in Bragg peaks as a function of temperature. These experiments place stringent requirements on the experimental setup. First, large Bragg angles are desired in order to minimize errors caused by misalignments of the sample or the incident x-ray beam. Second, high resolution in Bragg angle is necessary; therefore a vertical diffraction geometry is preferred because vertical beam collimation is better than horizontal beam collimation at synchrotron sources. In addition, thin films are typically strongly textured, constraining the geometries available for diffraction. Furthermore, a stage capable of both heating the sample and protecting it from the atmosphere is required. Finally, stresses relax during the hold at constant temperature at a rate that depends on the absolute stress and temperature. Therefore, acquiring diffraction peaks quickly is necessary to capture the initial stress state and any time-dependent relaxation behavior.

GI-RSMs can be used to characterize the structure of self-organized molecular films and supermolecular assemblies. GI-RSM methods were first developed to study molecular self-organization at an air-water interface[8] but have been recently extended to thin films of molecules adsorbed on glass or silicon substrates.[5] These experiments place a different set of requirements on the diffraction setup. By using a grazing incidence scattering geometry, the x-ray penetration depth is reduced so that the incident x-ray beam is mainly confined to the organic film, which decreases diffuse scattering and thus, background from the substrate. Furthermore the power density of the x-ray beam is reduced which is beneficial for sensitive samples such as organic thin films, which are prone to radiation damage. The GI-RMS measurements use the horizontal scattering geometry because the wider horizontal beam provides more photons for grazing incidence scattering geometries. Fast collection times are also important for the GI-RSM experiments, where typically small scattering intensities over large ranges in reciprocal space must be collected.

The thermomechanical and GI-RSM experiments led to the following general requirements: (1) access to any scattering vector above the sample horizon, (2) use of both vertical and horizontal diffraction geometries, (3) a heated sample stage capable of maintaining the sample in an oxygen-free environment, as well as the ability to mount a variety of standard sample stages, and (4) appropriate line and area detectors.

To meet these requirements we chose a "4S+2D" diffractometer design having four rotation axes in the κ geometry to control sample orientation and two rotation axes for orienting the detector. In a conventional four-circle diffractometer with a full χ ring, certain peaks are inaccessible because the x-ray beams are blocked by the χ ring (particularly for scattering vectors near the sample normal at high 2θ) and routing of power, cooling, vacuum, and signal lines around the χ ring to the sample stage over a wide range of angles is problematic. An open χ ring can help resolve peak accessibility problems but is more compliant. The κ goniometer allows access to all scattering vectors above the sample horizon in both vertical and horizontal diffraction geometries, leaves room for utility connections to the sample stage, and can meet stiffness requirements. The detector arm consists of a vertical rotation stage attached to a horizontal rotation stage and provides the ability to fully utilize both vertical and horizontal diffraction planes. The detector arm motion covers a majority of the hemisphere above the horizontal diffraction plane. Compared with other diffractometers designed to overcome similar constraints in surface diffraction—e.g., a five-circle diffractometer[9] in which a vertically scattering four-circle diffractometer was placed on a rotating table and a six-circle diffractometer[10] in which an additional arc was added to the detector arm of the five-circle diffractometer—the four circles controlling the sample orientation in our instrument are completely independent from the two circles controlling the detector, providing more flexibility in experimental setup. A 4S+2D six-circle diffractometer with similar degrees of freedom but using a conventional Eulerian cradle mounted on a vertical rotation axis for sample orientation was presented by You.[11] Our design is similar to the KM6 diffractometer produced by KUMA in the mid-1990s, as described by Thorkildsen *et al.*[12]

The new sample stage was designed primarily for the thin film thermomechanical strain measurements. This unique design minimizes variations in sample position with temperature due to thermal expansion. A z-translation motor is provided, which can be used to position the sample in the diffractometer's center of rotation and to actively correct for displacements due to thermal expansion if necessary. The sample is enclosed in a chamber which can be maintained in ultrahigh-vacuum (UHV) or inert or reducing atmospheres to prevent sample oxidation. X-ray access is provided by a beryllium dome and sample mounting clips that minimize interference with the x-ray beam.

The new detectors provide a means to collect data quickly. In particular, both the line detector and area detector are capable of capturing a complete diffraction peak simultaneously, which significantly decreases measurement time. This is advantageous both for the thermomechanical experiments in order to distinguish relaxation events and for the GI-RSM experiments, where typically small scattering intensities over large ranges in reciprocal space must be collected. Of course, higher sample throughput is highly advantageous at synchrotron sources with limited beam time.

In this article we describe the components of the new diffractometer system and present some of their technical characteristics. Some capabilities of the system are demonstrated in a discussion of thin film thermomechanical measurements of a bicrystal (011) Al film on a Si substrate and

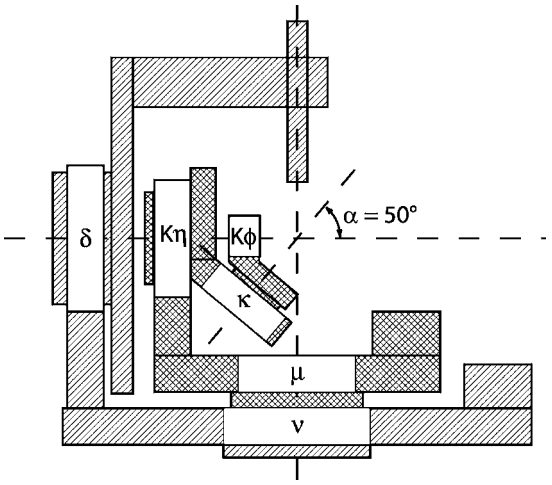

FIG. 1. Schematic representation of the six-circle κ diffractometer with all rotation axes lying in the plane of the page ($K\eta$=90°, κ=0°, $K\phi$ =arbitrary, μ=0°, ν=0°, δ=90°). The real rotation axes $K\eta$, κ, and $K\phi$ and the angle α_0 are used in Eqs. (1)–(3) to orient the sample using pseudo-goniometer-angles ω, χ, and ϕ representing the more common Eulerian geometry.

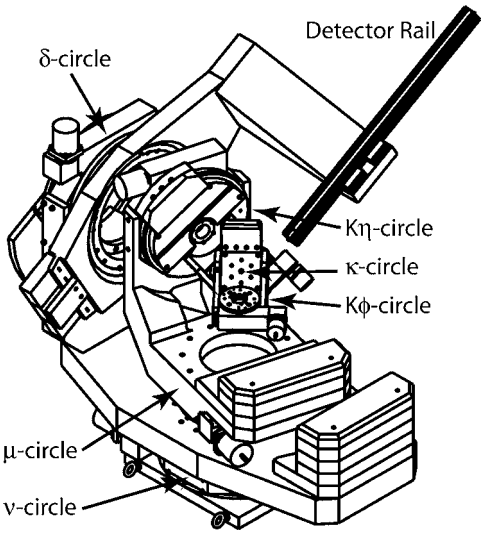

FIG. 2. Line drawing of the six-circle κ diffractometer at $K\eta$=57°, κ =134.8°, $K\phi$=arbitrary, μ=5°, ν=0°, and δ=45°. The κ goniometer leaves the area above the sample free so that, by suitable combinations of rotations, it is possible to access a wide range of reciprocal space without parts of the diffractometer obstructing incident or diffracted beams.

GI-RSM experiments on a ten layer octadecyl phenol Langmuir-Blodgett (LB) film on a Si substrate.

II. DESCRIPTION

The new diffractometer system was designed to work in the G2 experimental station. The G2 station uses an "x-ray transparent" Be (0002) monochromator/beam splitter to share an intense x-ray beam from a multilayer monochromator with the G3 experimental station. A range of incident beam energies between 8 and 16 keV is accessible. The Be crystal is used as a single side bounce monochromator operating in Laue transmission mode and diffracts a 0.1% energy bandpass of the beam from the multilayer mirror into the G2 station. The remaining beam that is not diffracted into the G2 station continues into the G3 station through a lead enclosed beam pipe.

A. Diffractometer

A schematic representation of the diffractometer with all rotation axes in a single plane is shown in Fig. 1. The diffractometer, designed and fabricated in collaboration with Advanced Design Consulting USA, Inc. (Lansing, NY), consists of six rotation stages, four for sample alignment and two for detector alignment. While at least one other naming convention and set of angle calculations has been presented,[12] the basic naming convention used by You[11] has been adopted here but has been adapted to include a κ goniometer, which is comprised of the inner three sample rotation stages, $K\phi$, κ, and $K\eta$. The fourth sample rotation, μ, is used as the θ rotation in horizontal diffraction mode and is used to align the diffractometer in vertical diffraction mode by making the $K\eta$ axis perpendicular to the incident x-ray beam. This alignment must be done when the beam energy is changed because the beam direction changes when the side bounce monochromator is used to change the energy. The two detector rotation stages, ν and δ, are independent of the sample rotation stages. When operating in vertical or horizontal diffraction mode, the δ or ν rotation, respectively, is used as the 2θ rotation. Both detector rotations can be used simultaneously to increase the coverage of reciprocal space. Figure 2 shows an accurate perspective drawing of the diffractometer with $K\eta$=57.0°, κ=134.8°, $K\phi$=arbitrary, μ =5.0°, ν=0°, and δ=45.0°.

All six rotation stages are driven by stepper motors and use microstepping. Rotations are controlled through SPEC (Certified Scientific Software, 2005) software on a computer running a Linux operating system. SPEC provides a geometry code for six-circle diffractometers based on algorithms given by You[11] and includes the κ-goniometer configuration. For simplicity, all sample rotations are calculated in Eulerian geometry[13] using three orthogonal pseudoaxes, η, χ, and ϕ. SPEC then translates the pseudorotations into real motor positions based on the following set of equations:[14]

$$K\eta = \eta - \arcsin[-\tan(\chi/2)/\tan(\alpha_0)], \quad (1)$$

$$K\phi = \phi - \arcsin[-\tan(\chi/2)/\tan(\alpha_0)], \quad (2)$$

$$\kappa = 2\arcsin[\sin(\chi/2)/\sin(\alpha_0)], \quad (3)$$

where α_0 is the angle between the $K\eta$ and κ axes and was specified to be 50°. Another description of this conversion, and the advantages of the κ geometry, was provided by Robinson *et al.*[15]

Material selection for the diffractometer design was influenced by two competing factors, a relatively large load from sample stages and the physical size of the G2 experimental station. The sample stage, details given below, has a stainless steel construction designed for UHV sample environments and weighs approximately 8 kg. With this load, high stiffness diffractometer components are required to prevent sample displacements from the center of rotation of the diffractometer. A target tolerance of 50 μm was established. Greater stiffness can be achieved with larger rotation stages

and stiffer materials. Although a steel construction would provide greater stiffness, it would also increase the total weight of the diffractometer and require even larger rotation stages. The physical size of the G2 experimental station creates an upper limit on the size of the diffractometer and therefore the size of the rotation stages and materials used for construction. All six rotation stages of varying sizes were manufactured by Huber Diffraktionstechnik GmbH & Co. KG (Rimsting, Germany) using aluminum alloy housings and provide excellent stiffness to weight ratios. Larger support structures were produced from cast aluminum alloy by Elmira Pattern and Foundry Co. (Elmira, NY) and smaller structures were machined from aluminum alloy plate stock.

To reduce sample displacements arising from elastic deflections of the diffractometer all rotation stages are counterbalanced with lead weights. The counterbalances put the center of gravity of the load on each rotation stage as close as possible to the center of the rotation bearings. Because loads on the three inner stages change significantly for different rotations, the counterbalances were designed to minimize the motion of the location of the center of gravity of the load on each rotation over the range of possible rotations.

The diffractometer was designed to be easy to set up and compatible with existing equipment. A working distance (the distance between the $K\phi$ interface plate and the center of rotation) of 129 mm was incorporated into the design to be consistent with other diffractometers at CHESS. Different detector assemblies are accommodated by using an easy-to-modify X48 precision rail system from Newport (Irvine, CA). The diffractometer is bolted to a motorized table that provides a convenient method to align the diffractometer with the incident x-ray beam. A three-point kinematic mount is used to position the table height, pitch, and roll. The diffractometer sits on top of horizontal Thompson rails and can be moved with a motorized lead screw to follow the x-ray beam when the energy is changed.

B. Sample stage

A schematic representation of the sample stage, also designed and fabricated in collaboration with Advanced Design Consulting USA, Inc (Lansing, NY), is shown in Fig. 3, where a cross-sectional view of the sample stage mounted on a rotation stage and a detailed view of the heater assembly are presented. A novel system was designed to minimize thermal expansion in a direction normal to the film surface (z direction) that also maintains a clear path for incident and diffracted x-ray beams. To prevent obstructions to the x-ray path from the assembly, the heater and a glass ceramic (Macor®) insulator were recessed into a copper support using thin positioning lips at the top surface of the heater and insulator. The positioning lips for the heater and insulator are 0.125 and 0.250 cm in thickness, respectively, which produces a minimal thermal displacement of 33 μm in the z direction over the total temperature range of the heater, room temperature to 900 °C. The Cu support is water cooled to minimize thermal displacements and provides a thermal conduction path when cooling a sample. Samples are held against the heater with clips that can be placed in different positions to avoid interference with the x-ray beams and are

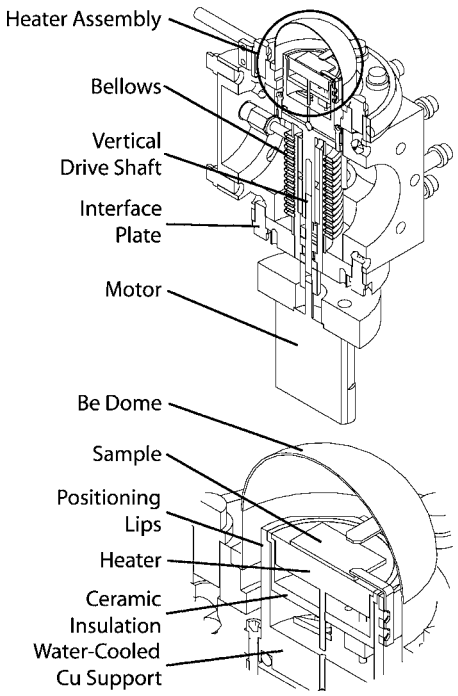

FIG. 3. (a) Schematic representation of the sample stage attached to the $K\phi$ rotation stage and (b) detailed view of the heater assembly. Samples can be heated up to 900 °C in UHV or controlled atmosphere. Sample displacements from thermal expansion can be corrected using a motorized z translation.

thermally isolated from the Cu support by glass ceramic spacers. The heating element was custom built by HeatWave Labs (Watsonville, CA), is 3.18 cm in diameter, and is constructed from a molybdenum shell with an alumina potting.

The heater assembly sits on a glass ceramic ball bearing on top of the vertical sample drive and is held in place by four adjustable screws. This attachment can be used like a two axis goniometer and allows the heater assembly to be adjusted to bring the sample normal parallel to the diffractometer $K\phi$ rotation axis. Translation in the z direction is motorized and consists of a finely threaded rod with precision slides that maintain alignment. The translation is driven by a stepper motor that is also controlled with the diffractometer software, SPEC. The threaded rod and slides are separated from the sample environment by a vacuum bellows.

The sample environment is enclosed within a stainless steel box measuring 8.59 cm per side with six conflat flange ports. The heater assembly puts the sample surface above the top flange and is capped with a beryllium dome (Brush Wellman, Inc., Fremont, CA) that was brazed to a conflat flange. The dome is 5.08 cm in diameter and allows all reflection geometries to be used during experiments. Sample exchange requires removing the dome to access the sample. A copper cooling tube is clamped to the conflat flange that is brazed to the beryllium dome to remove heat from the beryllium during a thermal cycle. The four ports around the sides of the cube provide feedthroughs to give access for thermocouples, electrical power to the heater, cooling water, and atmospheric controls. Four thermocouples are used to monitor the thermal profile of the heater, sample, insulator, and water-cooled Cu support. Thermocouple temperature readings are measured

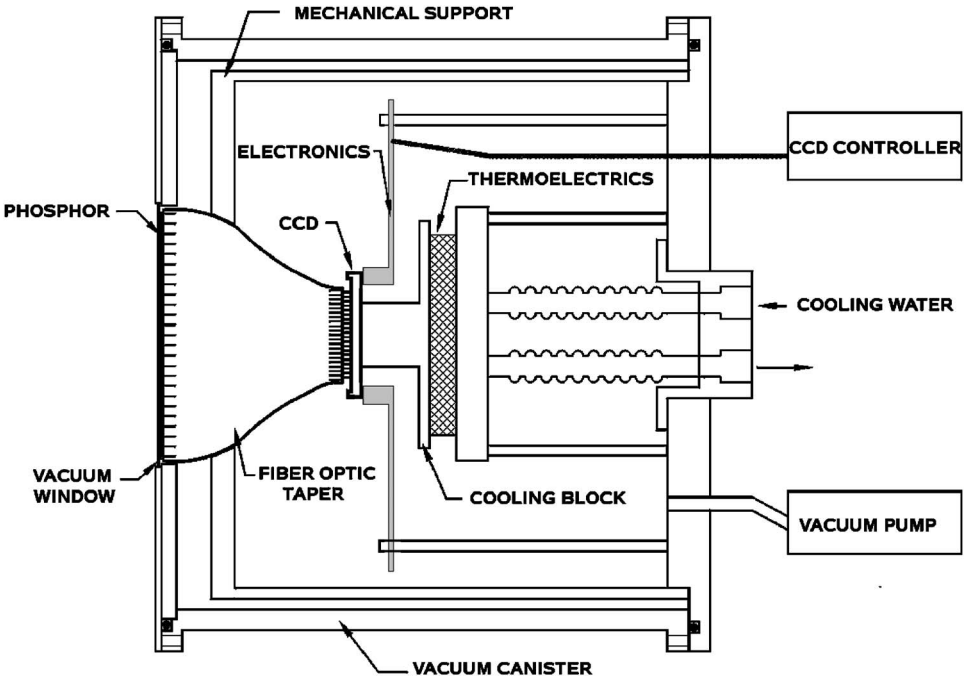

FIG. 4. Schematic representation of the area detector (Ref. 16). X rays incident on a thin phosphor sheet are converted to visible light. The fiber-optic taper efficiently reduces this visible light image onto the CCD which, in turn, records the image. The CCD is cooled via a thermoelectric assembly to reduce the noise associated with dark current.

with a digital multimeter and TCSCAN card (Keithley Instruments, Inc., Cleveland, OH). Power to the heater is controlled by a proportional-integral-derivative (PID) controller (Eurotherm, Inc., Leesburg, VA). A LABVIEW (National Instruments, Austin, TX) program was written in-house to remotely control and record temperatures. Cooling water for both the water-cooled Cu support and the beryllium dome was supplied by a recirculating chiller (Julabo USA, Inc., Allentown, PA). The flow rate through the water-cooled Cu support is 2.5 l/h. The sample atmosphere can be either a constant flow of forming gas (such as 900 ppm CO with balance N_2) or evacuated through a vacuum hose by turbomolecular and rotary vane pumps (Pfeiffer Vacuum, Nashua, NH). The sample stage can be bolted directly to the $K\phi$ rotation stage using a modified interface plate.

C. Detectors

Two new detectors were added to the G2 instrumentation, one area detector and one line detector. The area detector was built in-house based on a fiber-optic/charge-coupled-device (CCD) design;[16] a schematic representation of the detector is shown in Fig. 4. The detector works by converting x rays to visible light using a phosphor screen. A fiber-optic taper is used to demagnify the image produced on the phosphor screen and transmit it to a CCD where it is converted to a digital image. The primary component of this detector is a scientific-grade CCD, model KAF-1001E Blue-Plus from Eastman Kodak Company (Rochester, NY). The Blue-Plus CCD was selected because it has very high quantum efficiency for shorter wavelengths of light. In traditional CCDs, blue light is absorbed in the polysilicon electrodes on top of the light-sensitive silicon volume. This can be overcome by using thinned, back-illuminated CCDs, but these CCDs are delicate and expensive. The Blue-Plus CCD uses indium tin oxide electrodes to reduce absorption of blue light, resulting in a high quantum efficiency with front-side illumination. The CCD has 1024×1024 pixels with a pixel size of 24 μm. The CCD is optical-epoxy bonded to a fiber-optic taper (Incom, Inc., Charlton, MA) that has a 2.9:1 demagnification ratio, which gives a pixel size at the input face of the fiber optic of 69.8 μm. A CCD controller (Finger Lakes Instrumentation LLC, IMG-series, Lima, NY) was integrated with a cryostat made to hold the fiber-optic/CCD assembly. A gadolinium oxysulfide:Tb (P-43) screen (Grant Scientific, Gilbert, SC) made of phosphor powder settled onto aluminized Mylar at a density of about 15 mg/cm^2 was used. The phosphor screen is pressed against the fiber-optic taper face by vacuum capture between the face and an opaque plastic/aluminum composite film.

A 1100X linear position sensitive detector (PSD) was purchased from Ordela, Inc. (Oak Ridge, TN). The 1100X uses the delay line technique[17] to determine the location of an ionizing event along a wire anode 10 cm in length with an accuracy of 150 μm. Ionization occurs when a photon interacts with the Xe/CH_4 counting gas in the detector. Voltage pulses generated by the ionization event are preamplified and sent to a time-to-amplitude converter (Ordela, Inc, AIM-206). The pulse height signal is recorded by a multichannel analyzer (MCA) that bins each ionization event into one of 1024 channels corresponding to its position along the counting wire. The MCA is an Ortec (Oak Ridge, TN) TRUMP-PCI-2k PCI board in the station computer and communicates directly with the SPEC computer program. For handling and displaying the MCA data, the macro package MCA.MAC from the European Synchrotron Radiation Facility (ESRF) was used. For data analysis, each channel from the MCA is converted to an angle in 2θ based on a calibration of the PSD. Bias for the PSD is supplied by a 0–3 kV adjustable high voltage power supply, model NHQ103M from FAST ComTec GmbH (Oberhaching, Germany).

TABLE I. Pairs of axes in the κ diffractometer that are parallel or orthogonal.

Parallel	Orthogonal
δ and $K\eta$ for $\nu=\mu$	δ and ν
μ and ν	$K\eta$ and μ
$K\eta$ and $K\phi$ for $\chi=0°$	$K\eta$ and $K\phi$ for $\chi=90°$

III. TECHNICAL CHARACTERISTICS

A. Diffractometer

The six rotation axes were aligned to each other by a method described elsewhere.[18] The quality of the alignment was determined by measuring the sphere of confusion (SOC) and the angular deviation from parallelism or orthogonality for specific pairs of axes, given in Table I. The SOC was measured using a tooling ball attached to the $K\phi$ rotation stage and placed at the center of rotation (COR) of the diffractometer along with a dial indicator attached to the detector arm. The maximum deviation recorded by the dial indicator for all rotations about all six axes is less than 150 μm. However, rotations about the δ axis contribute the largest displacements because of compliance in the detector arm. With δ fixed, the maximum deviation for all rotations about the other five axes is less than 30 μm. Angular deviations were measured with a granite machinist's cube and the dial indicator. Deviations for all pairs of axes were less than 100 μrad. The tooling ball is 44 mm in diameter, has a roughness less than 1 μm, is made of SiC, and was purchased from Spheric-Trafalgar Ltd. (West Sussex, England). The granite cube is 7.62 cm per side and has an accuracy of 0.1 μm. The digital readout dial indicator has a precision of 1 μm and was purchased from Starrett (Athol, MA), model 2720-0.

The transformation between Eulerian space and κ space depends on the angle α_0 between the $K\eta$ and κ axes. Because of machining tolerances, the design angle of 50° cannot be guaranteed. Therefore, the angle between the axes was measured directly. One simple method that can be used to measure the angle is based on Eq. (3), rewritten here in terms of α_0:

$$\alpha_0 = \arcsin\left(\frac{\sin(\chi/2)}{\sin(\kappa/2)}\right). \tag{4}$$

Here we see that α_0 can be calculated by measuring the rotation about the κ axis for a known χ rotation. First, the granite cube and dial indicator were used to set the 0° position for κ (and χ), which is defined as $K\phi$ collinear to $K\eta$. Then, the cube and indicator were used to find the rotation for κ such that $K\phi$ is orthogonal to $K\eta$, which is defined as χ equals 90°.[13] Such a rotation in κ was found at 135.325°, which corresponds to an α_0 angle of 49.860°.

B. Sample stage

The thermal characteristics of the sample stage were determined over a temperature cycle up to 900 °C. Sample displacements caused by thermal expansion of the heater components were directly measured using x rays. Measurements were performed using a rotating anode source and a point detector (Bicron®, Saint-Gobain, Newbury, OH) aligned to the direct x-ray beam. The beam was well collimated with two sets of incident beam slits and two sets of detector slits. A sample was placed at the center of the x-ray beam, which is found by scanning the sample through the beam and finding the position at which half of the intensity at the detector is blocked by the sample. These scans were repeated at 100 °C intervals up to 900 °C. The change in half-intensity position as a function of temperature is shown in Fig. 5, top panel. Sample displacements over the thermal cycle are nonlinear with temperature and have a maximum displacement of 155 μm. Using this calibration, errors in the sample height due to thermal expansion can be actively corrected using the vertical sample drive during an experiment. The sample drive has a precision of better than 2 μm, as measured with a dial indicator.

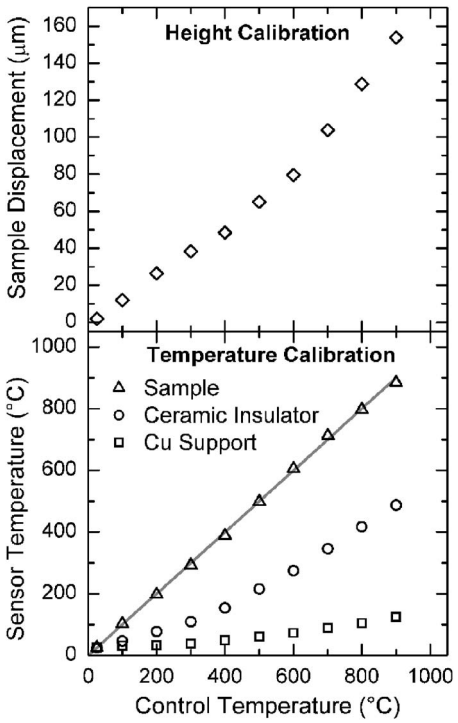

FIG. 5. Top panel: Height calibration of the sample stage during a thermal cycle. Sample displacements were determined at each temperature by scanning the sample through an x-ray beam and using the position at half the maximum intensity. Bottom panel: Temperature calibration of the sample stage during a thermal cycle. The thermocouple attached to the underside of the heating element was used as the control thermocouple. The gray line has a slope of 1.

The source of the thermal displacements can be easily identified by consulting the thermal profile of the heater components, Fig. 4, bottom panel. The temperatures at the sample, insulator, and water-cooled Cu support are given as a function of the temperature of the thermocouple bonded to the underside of the heating element, which was used as the feedback sensor for the PID controller. The sample temperature maintains a nearly 1:1 ratio with the heating element and the insulator provides a good thermal barrier to the water-cooled Cu support but still allows the support to reach 125 °C when the sample is at 900 °C. This change in tem-

TABLE II. Lattice planes with corresponding ψ and 2θ angles for planes in the [100] and $[01\bar{1}]$ zone axes that were measured for the $\sin^2(\psi)$ strain analysis.

[100] zone axis			$[01\bar{1}]$ zone axis		
Plane	ψ (deg)	2θ (deg)	Plane	ψ (deg)	2θ (deg)
(133)	13.26	103.29	(042)	18.43	107.13
(333)	35.26	138.39	(040)	45.0	92.04
(422)	54.74	123.61	$(04\bar{2})$	71.57	107.13
(511)	74.21	138.39			

perature of the Cu support contributes significantly to the total sample displacement in the z direction because of thermal expansion. The nonlinear behavior observed in the sample displacements can also be seen in the insulator and Cu support temperature profile. The cooling water temperature was maintained at 16 ± 2 °C over the entire thermal cycle. The beryllium dome temperature was also monitored and did not exceed 70 °C over the thermal cycle.

C. Detectors

The CCD detector was fully characterized using procedures described by Barna *et al.*[19] The detector has a sensitivity of 17 electrons/x ray at 8 keV with a read noise of 11 electrons. The read time is 4 s. The dark current was 0.08 electrons/pixel/s at the operating temperature of −40 °C.

IV. EXAMPLE APPLICATIONS

In this section, some capabilities of the new diffractometer system are presented using a strain analysis of a 1 μm bicrystal (011) Al film and reciprocal space mapping of a LB film for examples.

A. Thin film thermomechanical testing

The new diffractometer system facilitates high precision thermomechanical testing of textured thin films where stresses are determined using x-ray diffraction strain analysis methods at different temperatures. The strain analysis methods are typically based on the $\sin^2(\psi)$ technique using the ψ geometry.[20,21] In general, plane spacings d are measured at several different ψ angles, where ψ is the angle between the sample normal and the normal to the measured lattice planes. For certain stress states, crystal elasticity theory predicts that d will vary linearly with $\sin^2(\psi)$. By fitting a straight line to d vs $\sin^2(\psi)$ data, the spacing of planes whose normals lie in the surface plane can be determined. With the knowledge of the unstrained lattice parameter and elastic constants, the stress in the plane of the sample surface can be determined. For the six-circle κ diffractometer, the three sample pseudorotations (η,χ,ϕ) and one detector rotation (δ) are used for strain analysis. The incident and exit beam angles are equal such that $\eta=\delta/2$, the sample normal is collinear with ϕ, and $\chi=90°-\psi$.

An example strain analysis using the G2 diffractometer system was performed on a 1 μm bicrystal (011) Al film. The film was heteroepitaxially deposited on a single crystal (001) Si substrate by thermal evaporation following the method given in Ref. 22. Films deposited by this method have only two orientation variants: OR1, $(011)_{Al}[100]_{Al}\|(001)_{Si}[110]_{Si}$, and OR2, $(011)_{Al}[01\bar{1}]_{Al}\|(001)_{Si}[110]_{Si}$. Both orientations have (011) planes parallel to the film plane and are rotated by 90° to each other in the plane of the film. The microstructure is characterized by columnar, interlocking grains that form a mazed grain structure with no triple junctions. Following the method given by Nowak *et al.*,[4] stresses in the plane of the film were determined in two orthogonal crystallographic directions, [100] and $[01\bar{1}]$. The spacings between lattice planes of three sets of planes in the [100] zone axis of OR2 and four planes in the $[01\bar{1}]$ zone axis of OR1 were measured using Bragg diffraction. Measured plane spacings and corresponding ψ and 2θ angles (the wavelength of the incident x-ray beam was 0.1457 nm) are given in Table II. The Bragg peaks for most of these planes would not have been accessible using an Eulerian cradle. Because the orientation variants are rotated by 90°, spacings for lattice planes in the [100] and $[01\bar{1}]$ zone axes were measured in the same diffraction plane removing the necessity for a sample normal rotation that would be required in a single crystal. Lattice strains were calculated from the measured plane spacings and used to extrapolate strains in the [011], [100], and $[01\bar{1}]$ directions from linear fits to the two data sets, Fig. 6. Calculated strains are given in Table III along with stresses that were calculated using Hooke's law and single crystal elastic

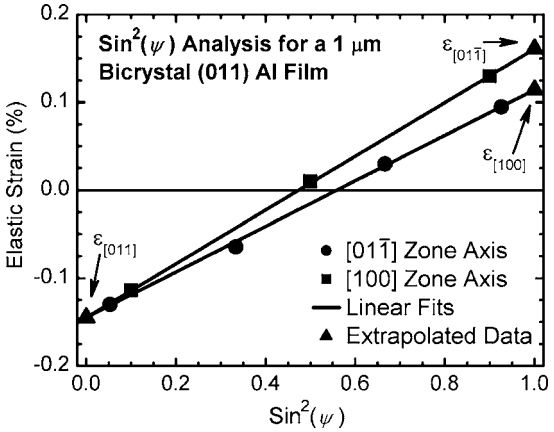

FIG. 6. $\sin^2(\psi)$ strain analysis for a 1 μm bicrystal (011) Al film. Strains and stresses based on this analysis are given in Table III. These stresses are reasonable and the strain resolution is better than 1×10^{-3}.

TABLE III. Strains and stresses determined for the three normal directions in a 1 μm bicrystal (011) Al film.

Direction	Strain (%)	Stress (MPa)
[011]	−0.145	0[a]
[100]	0.114	134
[01$\bar{1}$]	0.161	171

[a]The stress in the [011] direction is defined as zero in the method.

constants for Al.[23] With no corrections, film strains on the order of 1×10^{-3} can be easily measured. With a calibration of the δ rotation, the systematic errors caused by compliance in the detector arm can be identified and removed, improving the resolution. Other measurements of this type are discussed elsewhere.[4,24]

B. Grazing incidence-reciprocal space mapping

For the GI-RSM experiments, the experimental geometry is defined by four angles (α, β, ψ_s, and ϕ).[25] The angle between the incident beam and the sample surface, α, is set below the critical angle of the substrate. The exit angle β, also called the out-of-plane scattering angle, is measured along the line detector. The in-plane scattering angle is defined as ψ_s. (Note that ψ_s is typically just named ψ in surface diffraction experiments. We add the subscript here to distinguish it from the goniometer pseudoaxis ψ.) Finally, ϕ is the sample azimuth rotation, which can be used to align the substrate with the incident x-ray beam in samples that have preferred in-plane orientation. The sample is seated on a motorized height stage that precisely aligns the sample to the incident x-ray beam. Two diffractometer sample rotations (ϕ, η) and both detector rotations (δ, ν) are used in the GI-RSM geometry. The incident angle α is set using the $K\eta$ rotation, and the sample azimuth rotation ϕ is collinear with the $K\phi$ axis of the diffractometer. Using the reflection of a laser beam and a manual goniometer head (Huber 1003) it is ensured that the surface normal is parallel to the ϕ axis. The in-plane scattering angle ψ_s is set with the ν rotation, while the out-of-plane scattering angle β is measured on the line detector. The range of β can be augmented using the δ rotation of the detector arm. The remaining two diffractometer sample rotations, χ and μ, are fixed at 90° and 0°, respectively.

A reciprocal space map is generated by scanning the line detector in combination with an aperture-matched Soller collimator in ν. The line detector records a range of β angles for each ν position and the entire scan is converted into a reciprocal space map. An example map is given in Fig. 7 for a ten layer octadecyl phenol LB film on a Si substrate. The Langmuir-Blodgett technique allows a layer-by-layer deposition of amphiphilic molecules creating well-defined supramolecular assemblies. Octadecyl phenol molecules form double layers (head to head, tail to tail) on Si substrates. The molecules stand upright on the surface, as is evidenced by the lateral structure of the first order Bragg rod, around 17.4° in ψ_s. The intensity modulation along this Bragg rod is related to the large unit cell dimension perpendicular to the surface. The partial rings through the film's Bragg peaks indicate that the mosaic structure of the LB films is caused by fluctuations at the film/substrate interface and the internal interfaces of the layers.

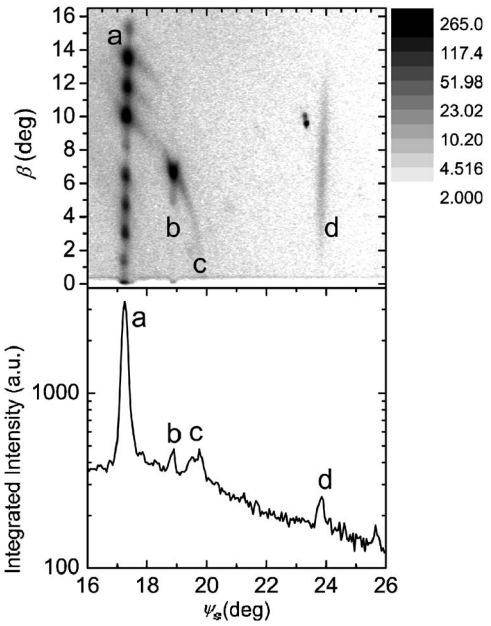

FIG. 7. Top panel: GI-RSM image from a ten layer octadecyl phenol Langmuir-Blodgett (LB) film; ψ_s is the in-plane scattering angle and β is the out-of-plane scattering angle. Bottom panel: A simulated in-plane powder diffraction scan derived from the GI-RSM. The intensity in β was integrated between 0° and 2° and plotted as a function of ψ_s. See text for an additional explanation.

The bottom panel in Fig. 7 shows a simulated result of an in-plane powder diffraction scan derived from the GI-RSM, where the intensity in β was integrated between 0° and 2° and plotted as a function of ψ_s. It can be clearly seen that the nature of features a–d can only be interpreted from the full GI-RSM: features a and b are scattering rods from the film. On rod b, only one Bragg peak has sufficient intensity to contribute in a significant way due to the molecule's form factor. Feature c is due to the mosaic structure associated with Bragg peak b. Finally the streak of intensity d appears to be a structureless scattering rod from the substrate.

At the time of writing we have applied the GI-RSM method to a large variety of samples, ranging from single-crystalline samples of molecular crystallites[5] to self-organized monolayers on GaAs surfaces[26] to surfaces of device-grade films of electro-optical materials[27] and fuel cell catalysts.[28] Grazing incidence scattering can be complemented with x-ray reflectivity and fluorescence methods[29] on the κ diffractometer, to offer a full spectrum of x-ray thin film analysis methods.

V. SUMMARY AND DISCUSSION

A new diffractometer system for the G2 experimental station was designed, constructed, and commissioned. The new system consists of a versatile six-circle κ diffractometer, an environmental- and temperature-controlled sample stage, an area detector, and a line detector. Key features of the new instrumentation include the following.

- Six-circle κ diffractometer: access to all scattering vectors above a sample's horizon, access to both horizontal and vertical diffraction geometries, compatible with existing sample stages, easy-to-modify experimental setups, and convenient lineup with incident x-ray beam.
- Sample stage: minimum sample displacements from thermal expansion, can actively correct for height errors induced by thermal expansion using a motorized stage, a very low oxygen atmosphere using either ultrahigh vacuum (UHV) or forming gas, and a temperature range up to 900 °C.
- Area detector: large coverage of reciprocal space, low noise, and good readout speed.
- Line detector: single photon counting for noise-free detection of low scattering signals, compatible with large illuminated sample area, when used in combination with the Soller collimator, and increases sample throughput by decreasing measurement time.

Combining these features provides an excellent system for thin film thermomechanical strain experiments and grazing incidence-reciprocal space mapping experiments for the characterization of organic thin films. Additionally, these features can easily be adapted to work with a wide range of other experiments and experimental setups.

ACKNOWLEDGMENTS

Support for this project was provided by the National Science Foundation through an Instrumentation for Materials Research Grant (DMR-0216881), by the Department of Energy (DE-FG02-02ER46001), and by Cornell University through the Cornell Center for Materials Research. This work is based upon research conducted at the Cornell High Energy Synchrotron Source (CHESS) which is supported by the National Science Foundation and the National Institutes of Health/National Institute of General Medical Sciences under Award No. DMR-0225180. Significant contributions were made by Joel Brock, Brian Clasby, Aaron Fleet, Jerry Houghton, Ted Luddy, Alan Pauling, and Dave Waterman. The authors would also like to thank the staffs of CHESS, Advanced Design Consulting, Inc., and SpaceMill Sciences Corp. The bicrystal (011) Al sample was provided by Daan-Hein Alsem (LBNL) and Eric Stach (Purdue University). The octadecyl phenol Langmuir-Blodgett film was provided by Oleg Konovalov (ESRF).

[1] M. A. Korhonen and C. A. Paszkiet, Scr. Metall. **23**, 1449 (1989).
[2] B. M. Clemens and J. A. Bain, Mater. Res. Bull. **17**, 46 (1992).
[3] R. P. Vinci, E. M. Zielinski, and J. C. Bravman, Thin Solid Films **262**, 142 (1995).
[4] D. E. Nowak, O. Thomas, and S. P. Baker (unpublished).
[5] D. M. Smilgies, D. R. Blasini, S. Hotta, and H. Yanagi, J. Synchrotron Radiat. **12**, 807 (2005).
[6] W. D. Nix, Metall. Trans. A **20A**, 2217 (1989).
[7] O. Kraft and C. A. Volkert, Adv. Eng. Mater. **3**, 99 (2001).
[8] J. Als-Nielsen, D. Jacquemain, K. Kjaer, F. Leveiller, M. Lahav, and L. Leiserowitz, Phys. Rep. **246**, 251 (1994).
[9] E. Vlieg, J. F. Vanderveen, J. E. Macdonald, and M. Miller, J. Appl. Crystallogr. **20**, 330 (1987).
[10] M. Lohmeier and E. Vlieg, J. Appl. Crystallogr. **26**, 706 (1993).
[11] H. You, J. Appl. Crystallogr. **32**, 614 (1999).
[12] G. Thorkildsen, R. H. Mathiesen, and H. B. Larsen, J. Appl. Crystallogr. **32**, 943 (1999).
[13] W. R. Busing and H. A. Levy, Acta Crystallogr. **22**, 457 (1967).
[14] D. E. Sands, *Vectors and Tensors in Crystallography* (Addison-Wesley, London, 1982).
[15] I. K. Robinson, H. Graafsma, A. Kvick, and J. Linderholm, Rev. Sci. Instrum. **66**, 1765 (1995).
[16] M. W. Tate, E. F. Eikenberry, S. L. Barna, M. E. Wall, J. L. Lowrance, and S. M. Gruner, J. Appl. Crystallogr. **28**, 196 (1995).
[17] C. J. Borkowski and M. K. Kopp, Rev. Sci. Instrum. **46**, 951 (1975).
[18] D. E. Nowak, Ph.D. dissertation, Cornell University, 2006.
[19] S. L. Barna, M. W. Tate, S. M. Gruner, and E. F. Eikenberry, Rev. Sci. Instrum. **70**, 2927 (1999).
[20] I. C. Noyan and J. B. Cohen, *Residual Stress Measurement by Diffraction and Interpretation* (Springer, New York, 1987).
[21] H. Behnken and V. Hauk, Thin Solid Films **193–194**, 333 (1990).
[22] N. Thangaraj, K. H. Westmacott, and U. Dahmen, Appl. Phys. Lett. **61**, 37 (1992).
[23] *Crystal and Solid State Physics*, Landolt-Börnstein New Series, Group III, edited by K. H. Hellwege and A. M. Hellwege (Springer, New York, 1966).
[24] D. E. Nowak, E. A. Stach, O. Thomas, and S. P. Baker (unpublished).
[25] D.-M. Smilgies, Rev. Sci. Instrum. **73**, 1706 (2002).
[26] C. McGuinness, D. R. Blasini, D.-M. Smilgies, and D. L. Allara (unpublished).
[27] D. R. Blasini, D.-M. Smilgies, S. Flores-Torres, H. D. Abruña, J. Slinker, J. Rivnay, and G. G. Malliaras (unpublished).
[28] D. R. Blasini, Y. Liu, D.-M. Smilgies, and H. D. Abruña (unpublished).
[29] D. R. Blasini, S. Flores-Torres, D.-M. Smilgies, and H. D. Abruna, Langmuir **22**, 2082 (2006).